Membrane penetration and trapping of an active particle

Abdallah Daddi-Moussa-Ider (iD), Segun Goh (iD), Benno Liebchen, Christian Hoell, Arnold J. T. M. Mathijssen (iD), Francisca Guzmán-Lastra, Christian Scholz, Andreas M. Menzel, and Hartmut Löwen

View Online   **Export Citation**   **CrossMark**

Membrane penetration and trapping of an active particle

View Online   Export Citation   CrossMark

Abdallah Daddi-Moussa-Ider,[1,a)] (iD) Segun Goh,[1] (iD) Benno Liebchen,[1] Christian Hoell,[1]
Arnold J. T. M. Mathijssen,[2] (iD) Francisca Guzmán-Lastra,[1,3] Christian Scholz,[1]
Andreas M. Menzel,[1] and Hartmut Löwen[1,b)]

AFFILIATIONS

[1] Institut für Theoretische Physik II: Weiche Materie, Heinrich-Heine-Universität Düsseldorf,
   Universitätsstraße 1, 40225 Düsseldorf, Germany
[2] Department of Bioengineering, Stanford University, 443 Via Ortega, Stanford, California 94305, USA
[3] Facultad de Ciencias, Universidad Mayor, Ave. Manuel Montt 367, Providencia, Santiago de Chile, Chile

Note: This article is part of the Special Topic "Chemical Physics of Active Matter" in J. Chem. Phys.
a) Electronic mail: abdallah.daddi.moussa.ider@uni-duesseldorf.de
b) Electronic mail: hartmut.loewen@uni-duesseldorf.de

ABSTRACT

The interaction between nano- or micro-sized particles and cell membranes is of crucial importance in many biological and biomedical applications such as drug and gene delivery to cells and tissues. During their cellular uptake, the particles can pass through cell membranes via passive endocytosis or by active penetration to reach a target cellular compartment or organelle. In this manuscript, we develop a simple model to describe the interaction of a self-driven spherical particle (moving through an effective constant active force) with a minimal membrane system, allowing for both penetration and trapping. We numerically calculate the state diagram of this system, the membrane shape, and its dynamics. In this context, we show that the active particle may either get trapped near the membrane or penetrate through it, where the membrane can either be permanently destroyed or recover its initial shape by self-healing. Additionally, we systematically derive a continuum description allowing us to accurately predict most of our results analytically. This analytical theory helps in identifying the generic aspects of our model, suggesting that most of its ingredients should apply to a broad range of membranes, from simple model systems composed of magnetic microparticles to lipid bilayers. Our results might be useful to predict the mechanical properties of synthetic minimal membranes.

Published under license by AIP Publishing. https://doi.org/10.1063/1.5080807

I. INTRODUCTION

Biological membranes play a crucial role in a large variety of cellular processes and serve as a barrier to protect the interior of living cells from unwanted agents and harmful external influences.[1-7] The interaction between particles and cell membranes is of crucial importance in a variety of biomedical applications, including targeted phototherapy, intracellular imaging, and diagnostic assays.[8-10] Once injected into a living organism, particle uptake can be achieved via passive mechanisms[11-15] or can be mediated by active processes

involving cellular energy input.[16-19] Considerable research advances have been made over the last few years in understanding the penetration of particles into cell membranes. Previous studies have shown that the particle uptake by living cells is strongly affected by the particle properties[20-24] and the physicochemical and functional properties of the membrane.[25-30]

As a simple framework for studying basic mechanisms of cell penetration, artificial model membranes provide a basis for understanding the complex interactions within living cells. For example, the formation of a desired target membrane

structure can be driven by an entropic mechanism[31] or can be achieved using controlled external fields.[32–37] In particular, self-assembled colloidal membranes have offered a novel framework for studying fundamental physical problems, such as geometric frustration in artificial spin-ice systems,[38–40] and can conveniently be built from isolated microparticles with adjustable interactions.[41–49] For this purpose, various types of interparticle interactions could be exploited, among which magnetic attraction stands out.

One possibility is to construct membranes from colloidal magnetic particles that, in other situations, serve as building blocks of magnetically self-assembled chains and sheets. Magnetic nanoparticles (MNPs)[50,51] are well-established nanocomponents, owing to their diverse promising technological and biomedical applications. Notable examples include their potential use as drug delivery agents[52–54] or as mediators to convert electromagnetic energy into heat (hyperthermia).[55] By binding MNPs to the surface of living cells, the membrane mechanical properties can conveniently be tuned by an external magnetic field.[56–58] Furthermore, magnetic colloidal and nanoparticles have proved to be useful in the design of optical stimuli-responsive materials[59–62] and in the development of artificial self-propelling active microswimmers.[63–77] Meanwhile, the dynamical properties of self-propelled active polymers and filaments have been investigated.[78–81] Additional studies include the dynamics of semiflexible polymer chains in the presence of nanoparticles[82] and the behavior of polymers in a crowded solution of active particles.[83]

Here, we develop a minimal model for a (non-fluctuating) membrane made of dipolar (e.g., electric or magnetic) particles sterically interacting with a constantly driven "active" particle.[84–92] This particle may represent, e.g., a swimming microorganism[68,69] or a synthetic micro- or nanomachine that can be manipulated under the action of controlled external fields.[93–96] Here, we focus on the case in which the persistence length of the trajectory of the active particle is large compared to its initial distance from the membrane, i.e., the particle essentially moves along a straight line towards the membrane.

In general, active particles can reach normally inaccessible areas inside living organisms and can perform delicate and precise tasks, holding great promise for prospective biomedical applications such as precision nanosurgery[97–99] or transport of therapeutic substances to tumor and inflammation sites.[100–102] Direct experimental observations have recently demonstrated the self-driven motion of acoustically powered active nanorods inside living HeLa cells.[103] These nanomotors have been shown to bump into cell organelles and exhibit directional motion and spinning inside the cells. A detailed modeling of the interactions of active particles and (cell) membranes may help to shed light on our understanding of the processes driving particle motion in living and synthetic cell components. Additionally, a fundamental understanding of these processes helps to improve the controllability of micro- and nanoparticle-based agents in complex environments. Potentially, this might be relevant for novel therapeutic drug targets for health therapy. One step in this direction

has been taken recently specifically for self-propelled particles interacting with a moving potential interpreted as a semipermeable membrane,[104] identifying an enhanced particle accumulation in front of the membrane accompanied with an increased drag force. Experimentally, the mechanical pressure exerted by a set of both passive isotropic and self-propelled polar disks onto flexible unidimensional model membranes has been studied.[105]

In the present work, we investigate a membrane model self-assembled from dipolar spheres arranged along a chain in the two-dimensional space. Their dipole moment can arise either from an unscreened magnetic or electric moment or from screened short-ranged electric interactions, also arising from polar colloidal clusters.[106] It has previously been shown that a chain of magnetic particles can exhibit intrinsic mechanical properties reminiscent of elastic strings or rods[107–112] depending on the additional particle interactions. In colloidal suspensions, magnetic interactions often cause flocculation due to the strong attraction at short distances.[113] Such effects are usually counterbalanced by repulsive steric interactions that prevent overlapping particle volumes at finite concentrations.[114–116] Additional elastic interactions may be considered in the form of harmonic springs. Particle systems subject to combinations of magnetic, steric, and elastic interactions have widely been utilized as a model system for ferrofluids and ferrogels.[117–126]

Using our simple model membrane as a basis to study the penetration process by a self-driven particle (moving under the action of a constant driving force), we obtain dynamical state diagrams indicating trapping and penetration states. We further observe penetration events with or without subsequent healing of the membrane depending on the range of the interactions between the membrane particles. Considering a chain of dipolar spheres, we derive a continuum theory[125,127] and we probe the particle displacement and dipole reorientation caused by the self-driven particle in the small-deformation regime. Good quantitative agreement is found between the theoretical results and numerical simulations.

The remaining part of the paper is organized as follows: in Sec. II, we present the system setup and derive from the potential energy the governing equations for the displacement and orientation fields of the dipolar spheres. We then present in Sec. III state diagrams indicating the possible steady configurations of the system. Moreover, we probe the transition between the dynamical states. In Sec. IV, we devise a linearized analytical theory that describes the temporal evolution of the membrane and we provide solutions for the trapping state in Sec. V. Concluding remarks are contained in Sec. VI.

II. SYSTEM SETUP

We consider in two spatial dimensions a simple model membrane composed of a chain of N identical dipolar particles of radius a and dipole moment $\boldsymbol{m}$. Here, we assume that the dipole moments rotate rigidly with the particles. The

membrane is fully immersed in a Newtonian viscous fluid of constant dynamic viscosity η. We support the chain at its extremities such that the particles on both ends are fixed in space. Moreover, we neglect Brownian noise, which should play only a minor role when considering a large membrane and large self-driven particles or systems at low temperatures. In the resulting equilibrium configuration, the dipolar particles are uniformly distributed along the chain and aligned along the x direction (Fig. 1). We denote by h the interparticle distance, initially set identical for all particles, and by $L = hN$ the total length of the chain.

A. Potential energy of the membrane

Next, we assume that the membrane particles are subject to three types of mutual interactions, namely, dipolar, steric, and elastic interactions. Accordingly, the system potential energy governing the time evolution of the membrane can be written as
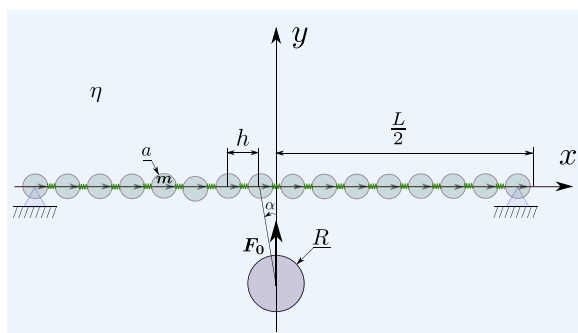
$$\mathcal{U} = \mathcal{U}_M + \mathcal{U}_S + \mathcal{U}_E, \tag{1}$$

where $\mathcal{U}_M$, $\mathcal{U}_S$, and $\mathcal{U}_E$ are contributions stemming from the dipolar, steric, and elastic interactions, respectively. In this study, we neglect for simplicity the fluid-mediated hydrodynamic interactions between the particles.

In the following, $\boldsymbol{m}_i$ denotes the dipole moment of the ith membrane particle, $i = 1, \ldots, N$. It is assumed that the magnitudes of the dipole moments are equal and constant for all the membrane particles, $m = |\boldsymbol{m}_i|$. Then, the dipolar part of the potential energy may be expressed as[128]

$$\mathcal{U}_M = \frac{\mu_0 m^2}{4\pi} \sum_{\substack{i,j=1 \\ j<i}}^{N} \frac{1}{r_{ij}^3} \big(\hat{\boldsymbol{m}}_i \cdot \hat{\boldsymbol{m}}_j - 3(\hat{\boldsymbol{m}}_i \cdot \hat{\boldsymbol{r}}_{ij})(\hat{\boldsymbol{m}}_j \cdot \hat{\boldsymbol{r}}_{ij})\big), \tag{2}$$

where μ_0 is the magnetic vacuum permeability, $\hat{\boldsymbol{m}}_i = \boldsymbol{m}_i/m$ gives the orientation of the ith dipole moment, $\boldsymbol{r}_{ij} = \boldsymbol{r}_i -$

$\boldsymbol{r}_j$ denotes the distance vector from particle j to particle i, $r_{ij} = |\boldsymbol{r}_{ij}|$ is its magnitude, and $\hat{\boldsymbol{r}}_{ij} = \boldsymbol{r}_{ij}/r_{ij}$ stands for the corresponding unit vector.

In order to avoid aggregation of the dipolar particles, we consider a repulsive Weeks–Chandler–Andersen (WCA) pair potential. The corresponding potential energy reads[129]

$$\mathcal{U}_S = 4\epsilon \sum_{\substack{i,j=1 \\ j<i}}^{N} N_{ij} \left(\frac{\sigma}{r_{ij}}\right)^6 \left(\left(\frac{\sigma}{r_{ij}}\right)^6 - 1\right) + \epsilon, \tag{3}$$

where we have defined the shorthand notation $N_{ij} = H(r_C - r_{ij})$, with $H(\cdot)$ being the Heaviside step function and $r_C = 2^{1/6}\sigma$ denoting a cutoff radius beyond which the potential energy is set to zero. Here, $\sigma = 2a$ is the particle diameter and ϵ is an energy scale associated with the hardness of the potential.

In addition, we allow for harmonic elastic-like interactions among adjacent particles. These interactions are included such as springs of constant stiffness k and rest length r_0. The corresponding potential energy is given by

$$\mathcal{U}_E = \frac{k}{2} \sum_{i=1}^{N-1} (r_{i,i+1} - r_0)^2. \tag{4}$$

Consequently, the resulting force and torque acting on the ith sphere are calculated from the system potential energy as[66] $\boldsymbol{F}_i = -\partial\mathcal{U}/\partial\boldsymbol{r}_i$ and $\boldsymbol{T}_i = -\hat{\boldsymbol{m}}_i \times (\partial\mathcal{U}/\partial\hat{\boldsymbol{m}}_i)$. We obtain

$$\begin{aligned}
\boldsymbol{F}_i = \frac{3\mu_0 m^2}{4\pi} \sum_{\substack{j=1 \\ j\neq i}}^{N} \frac{1}{r_{ij}^4} &\big((\hat{\boldsymbol{m}}_j \cdot \hat{\boldsymbol{r}}_{ij})\hat{\boldsymbol{m}}_i + (\hat{\boldsymbol{m}}_i \cdot \hat{\boldsymbol{r}}_{ij})\hat{\boldsymbol{m}}_j \\
&+ (\hat{\boldsymbol{m}}_i \cdot \hat{\boldsymbol{m}}_j)\hat{\boldsymbol{r}}_{ij} - 5(\hat{\boldsymbol{m}}_i \cdot \hat{\boldsymbol{r}}_{ij})(\hat{\boldsymbol{m}}_j \cdot \hat{\boldsymbol{r}}_{ij})\hat{\boldsymbol{r}}_{ij} \\
&+ 48\epsilon \sum_{\substack{j=1 \\ j\neq i}}^{N} N_{ij} \left(\frac{\sigma}{r_{ij}}\right)^6 \left(\left(\frac{\sigma}{r_{ij}}\right)^6 - \frac{1}{2}\right)\frac{\hat{\boldsymbol{r}}_{ij}}{r_{ij}} + k \sum_{\substack{j=i-1 \\ j\neq i}}^{i+1} \left(\frac{r_0}{r_{ij}} - 1\right)\boldsymbol{r}_{ij}
\end{aligned} \tag{5}$$

and

$$\boldsymbol{T}_i = -\frac{\mu_0 m^2}{4\pi} \sum_{\substack{j=1 \\ j\neq i}}^{N} \frac{\hat{\boldsymbol{m}}_i \times \boldsymbol{c}_{ij}}{r_{ij}^3}, \tag{6}$$

where we have defined, for convenience, the dimensionless vector $\boldsymbol{c}_{ij} = \hat{\boldsymbol{m}}_j - 3(\hat{\boldsymbol{m}}_j \cdot \hat{\boldsymbol{r}}_{ij})\hat{\boldsymbol{r}}_{ij}$.

B. Dynamical equations

Assuming low-Reynolds-number hydrodynamics,[130] the moments of the particle velocities are related to the moments of the hydrodynamic forces acting on them via the mobility functions.[131,132] Neglecting mutual hydrodynamic interactions between the particles yields

$$\boldsymbol{V}_i = \mu\big(\boldsymbol{F}_i + \boldsymbol{F}_i^{ext}\big), \qquad \boldsymbol{\Omega}_i = \gamma\,\boldsymbol{T}_i, \tag{7}$$

where $\boldsymbol{V}_i$ and $\boldsymbol{\Omega}_i$ denote the linear and angular velocities of the ith membrane particle, respectively. Here, $\mu =$

FIG. 1. Illustration of the system setup. Under the action of an effective propulsion force $\boldsymbol{F}_0$, a solid spherical particle of radius R approaches a membrane composed of N identical magnetic spheres of radius a and dipole moment $\boldsymbol{m}$. The membrane particles are initially equidistant with distance h from one another. We denote by L the total length of the membrane. The particles composing the membrane are subject to dipolar, steric, and elastic interactions. The system is immersed in a bulk liquid of constant dynamic viscosity η.

$1/(6\pi\eta a)$ and $\gamma = 1/(8\pi\eta a^3)$ are the translational and rotational mobilities for a sphere as given by the Stokes formulas, respectively. Moreover, $\mathbf{F}_i^{\text{ext}}$ is the external force resulting from the steric interaction with the self-driven particle that is moving under the action of a constant driving force $\mathbf{F}_0 = F_0\,\hat{\mathbf{e}}_y$. Here, we assume that the self-driven spherical particle of radius R interacts with membrane particles via the same soft repulsive WCA pair potential stated by Eq. (3) for $\sigma = a + R$.

Then, the equation of motion for the translational degrees of freedom reads

$$\frac{d\mathbf{r}_i}{dt} = \mathbf{V}_i. \tag{8}$$

Similarly, the equation governing the temporal evolution of the orientation of the ith particle is given by

$$\frac{d\hat{\mathbf{m}}_i}{dt} = \mathbf{\Omega}_i \times \hat{\mathbf{m}}_i, \tag{9}$$

which can be rewritten as

$$\frac{d\hat{\mathbf{m}}_i}{dt} = \frac{\gamma\mu_0 m^2}{4\pi} \sum_{\substack{j=1 \\ j\neq i}}^{N} \frac{1}{r_{ij}^3}\left(\left(\hat{\mathbf{m}}_i \cdot \mathbf{c}_{ij}\right)\hat{\mathbf{m}}_i - \mathbf{c}_{ij}\right), \tag{10}$$

by making use of Eqs. (6) and (7).

Considering now two-dimensional orientation vectors in the (xy) plane, the particle orientations are represented in the Cartesian basis system as $\hat{\mathbf{m}}_i = (\cos\phi_i, \sin\phi_i)$ with the angle ϕ_i measured relatively to the x direction. Furthermore, the angular velocity vector then possesses only one single component (along the z direction). Hence, the temporal evolution of the orientation angle of the ith particle is calculated as

$$\frac{d\phi_i}{dt} = \mathbf{\Omega}_i \cdot \hat{\mathbf{e}}_z = \gamma(\mathbf{T}_i \cdot \hat{\mathbf{e}}_z). \tag{11}$$

We now introduce an additional cutoff length $\ell = 3h/2$ for the dipolar and elastic interactions. That is, we multiply a Heaviside function of the form $H(\ell - r_{ij})$ to Eqs. (5) and (6). Accordingly, these interactions are now truncated beyond next-nearest neighbors. Such a cutoff can be reasonable for screened electric dipolar interactions. This assumption does not significantly change our results except for the membrane destruction state of absent-healing (see below), the occurrence of which hinges on the cutoff.

III. STATE DIAGRAM

As an initial configuration of the membrane, the interparticle distance h is taken equal to the cutoff radius r_C beyond which the steric forces vanish. Moreover, we assume that the rest length of the springs is equal to this initial interparticle equilibrium distance, i.e., $r_0 = 2^{7/6}a$.

Our parameter space has four essential dimensions. The two dimensionless numbers

$$E_1 = \frac{\mu_0 m^2}{4\pi a^3 \epsilon}, \qquad E_2 = \frac{aF_0}{\epsilon} \tag{12}$$

quantify the importance of the attractive dipolar force $(\sim\mu_0 m^2/a^4)$ and of the active force F_0 relative to the repulsive

steric force $(\sim\epsilon/a)$ at particle contact, respectively. These two parameters will be denominated as reduced dipole strength and reduced activity, respectively. One additional dimensionless number

$$\kappa = \frac{\pi}{6}\frac{kh^5}{\mu_0 m^2} \tag{13}$$

corresponds to the ratio of the elastic to the dipolar interactions. Moreover, we define the dimensionless number

$$\delta = \frac{R}{a} \tag{14}$$

as the ratio of the radius of the active particle relative to that of the membrane particle. The parameters κ and δ will be denominated as reduced stiffness and size ratio, respectively. For future reference, we also introduce a dimensionless number quantifying the ratio of the driving and dipolar forces in the form

$$P_0 = \frac{1}{12}\left(\frac{h}{a}\right)^4 \frac{E_2}{E_1}. \tag{15}$$

The latter will serve as our key control parameter discriminating trapped from penetrating states as detailed below. We note that $h/a = 2^{7/6}$ is kept constant such that P_0 is fully determined from the ratio E_2/E_1.

In Fig. 2, we present state diagrams identifying the possible dynamical states of the system in the plane of the two control parameters E_1 and E_2. The diagrams are constructed by numerical integration of the dynamical equations of motion using the 4th-order Runge-Kutta scheme with adaptive time step.[133] Results are shown for three values of the reduced stiffness κ which span a wide range of values to be expected in various situations. Here, we set $N = 20$ and $\delta = 1$. We have tested the robustness of the state diagrams by varying the number of membrane particles and have found no qualitative difference. Depending on the combination of the relevant control parameters, the self-driven particle either penetrates or remains in direct contact with the membrane (trapping state). In the latter case, the particle is essentially held back due to the steric interactions with the membrane particles. Furthermore, two penetration regimes are identified depending on whether the membrane self-heals and recovers its initial undeformed shape (red triangles) or remains damaged after the particle reaches the other side [green disks in (c)]. Qualitatively, penetration scenarios are observed for higher values of P_0 that indicate larger driving forces or smaller restoring dipolar forces than those in the trapped state. For $\kappa \gg 1$, penetration happens when

$$\frac{P_0}{\kappa} = \frac{2F_0}{kh} \gtrsim 1, \tag{16}$$

i.e., when the active force is larger than the overall elastic and dipolar restoring forces of a membrane particle with its two neighbors. After membrane penetration, self-healing always occurs for non- or weakly elastic membranes, for the
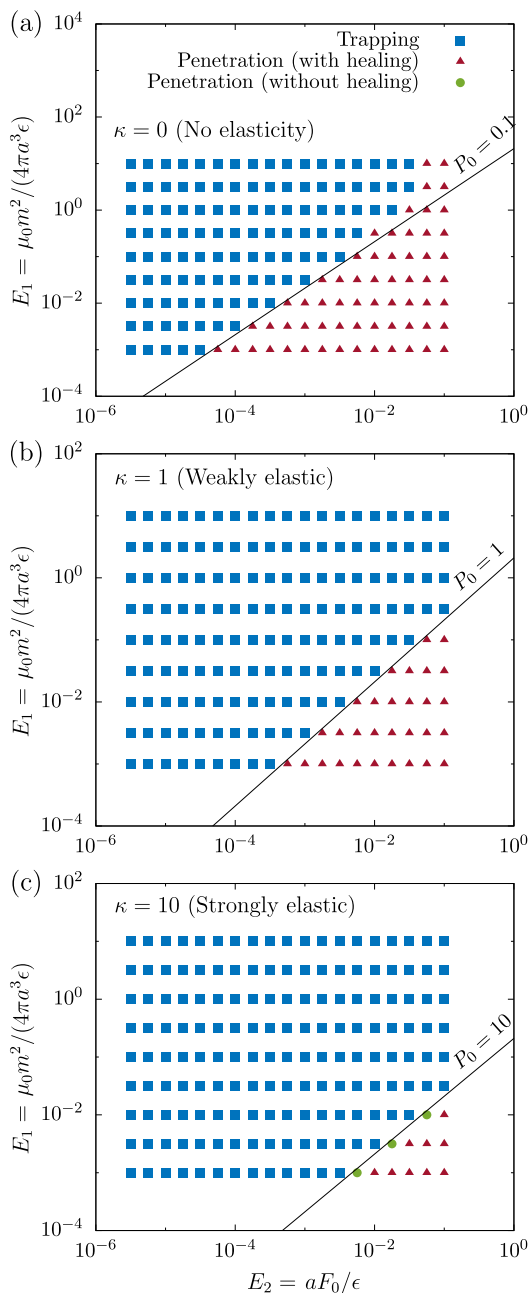
FIG. 2. Ability of penetration or trapping as a function of elasticity. Shown are state diagrams for (a) $\kappa = 0$, (b) $\kappa = 1$, and (c) $\kappa = 10$. Symbols represent the final states obtained from numerical integration of the dynamical equations, given by Eqs. (5)–(11). Here, membranes consisting of $N = 20$ dipolar particles have been examined and we set the size ratio $\delta = 1$. Depending on the values of the dimensionless numbers E_1 and E_2, the active particle is either trapped (blue squares) or passes through the membrane to reach the other side. After full penetrations, the membrane either shows a self-healing ability (red triangles) or remains permanently damaged (green disks). The latter behavior is only observed in the case of strongly elastic membranes shown in (c) for the present set of parameters. The solid lines display the estimates of the transition line between the states.

present set of parameters. In contrast to this, the membrane may remain permanently damaged for strongly elastic membranes, see Fig. 2(c). Besides, the elastic interactions cause a noticeable "shifting" of the transition line between the penetration and trapping states. Apart from this, they do not qualitatively alter our results and will therefore be omitted in most of our later calculations. It is worth noting that the detailed form of the steric repulsion may not be important as long as the reduced dipole strength $E_1 \ll 1$. An alternative could be the use of hard-core interactions. However, a softer potential is adopted here for numerical convenience to prevent the interparticle forces from diverging during the evolution dynamics.

We now describe the dynamical scenarios of the trapped and penetrating states depicted in Fig. 3. First, we examine the time evolution of membrane configurations. At the initial stage of the dynamics, the active particle pushes the membrane and subsequently bends the membrane, as shown in Figs. 3(a), 3(c), and 3(e). If the active force is strong enough ($P_0 \gg 1$), such deformation persistently increases and induces a growing distance between the two center particles of the chain, giving rise to a weakening of their mutual dipolar attraction. Consequently, the active particle penetrates through the membrane, see Figs. 3(c) and 3(e). Depending on the size of the active particle relative to that of the membrane particles, the membrane either closes again to recover its initial aligned configuration [self-healing behavior shown in (c) for $\delta = 1$] or remains permanently deformed [as shown for $\delta = 5$ in (e)]. In addition, we observe that the penetration event is also accompanied by a slight abrupt increase in the particle speed [small cusp occurring in (d) at $t/t_S \simeq 0.6$ and in (f) at $t/t_S \simeq 1.6$]. This small augmentation of speed is due to the steric interactions which support the particle motion at this final stage when the penetrated particle is sterically repelled by the nearby membrane particles. In sharp contrast, when $P_0 \ll 1$, the membrane develops a triangular profile, reaching a steady state without allowing the self-driven particle to pass, see Fig. 3(e). This trapping behavior is investigated in more detail in Secs. IV and V. Meanwhile, both scenarios can also be understood in terms of the velocity profiles of the self-driven particle presented in Figs. 3(b), 3(d), and 3(f). Since the dynamics are overdamped, the velocity can be interpreted as the total net force exerted on the particle. Accordingly, membrane penetration occurs when the external driving force remains larger than the membrane restoring forces.

In order to explore the membrane behavior in the penetration state in more detail, we present in Fig. 4 a state diagram in the parameter space (δ, E_2). Here, we keep the other parameters fixed at $\kappa = 0$, $E_1 = 10^{-2}$, and $N = 20$. We observe that the transition between the trapping and penetration states can only be enabled by increasing the reduced activity E_2, regardless of the size ratio δ. However, the latter strongly affects the membrane behavior in the penetration scenario. In the considered range of parameters, lower values of δ lead to self-healing, while larger values imply permanent damage of the membrane. The observed suppression of the healing behavior for large enough penetrating particles can be
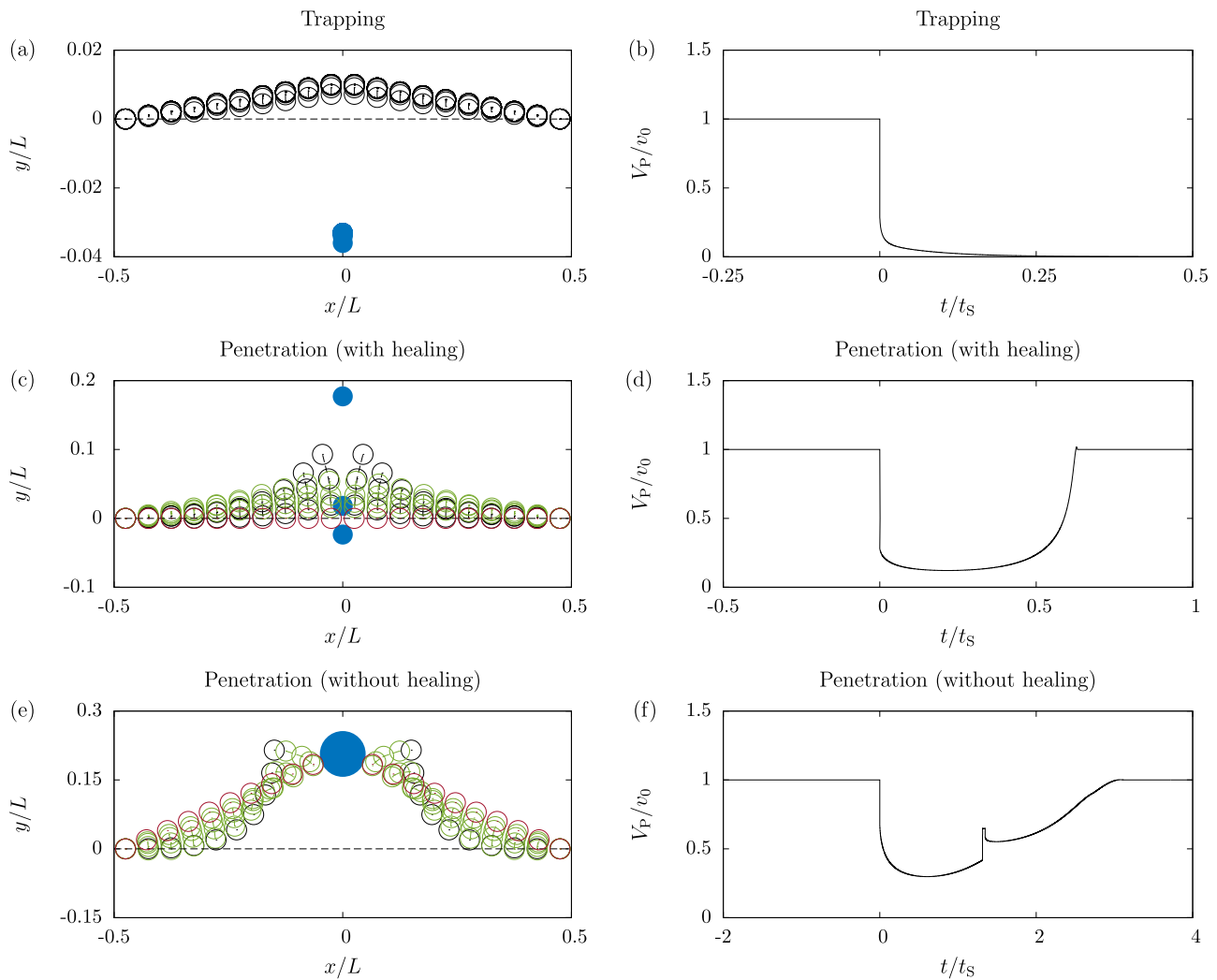
FIG. 3. Membrane dynamics of trapping and penetration states. (a) Frame series in the trapping state for $N = 20$, $\kappa = 0$, $\delta = 1$, $E_1 = 1$, and $E_2 = 10^{-2}$. Here, the frames are displayed every $0.2t_S$, where $t_S = \eta L^3/\epsilon$ is the simulation time unit. (b) Time evolution of the translational velocity of the active particle in the trapping state. (c) Frame series of the membrane conformation during the penetration state with healing, using the same set of parameters as in (a), except for $E_1 = 0.1$. The frames are displayed in time every $0.6t_S$. The black and green circles represent the positions of the membrane particles before and after the active particle (blue disk) reaches the upper side, respectively. As shown, the membrane recovers its original conformation after the active particle has passed (red circles). Panel (d) shows the corresponding translational velocity of the active particle versus time. (e) Frame series of the membrane shape during the penetration state without healing, using the same parameters as in (c), except for $R = 5a$. The frames are displayed every $6t_S$ in time with the same color as in (c). Circles shown in red represent the steady positions of the membrane particles. Panel (f) displays the corresponding time evolution of the active particle. We note that the particles in (a), (c), and (e) are not plotted to scale. Accordingly, the shown circles and disks only correspond to the positions of the centers of the particles. [The membrane particles and the driven particle in (a) are actually in contact, but the scales on the ordinate and abscissa are pronouncedly different.] Time $t = 0$ in (b), (d), and (f) corresponds to the moment when the active particle and the membrane begin to mutually interact.

understood by the fact that the mutual distance between the two central beads becomes larger than the cutoff distance ℓ, which could represent the average distance between cytoskeletal cross-linkers for biological membranes. If these links are broken by large active particles, the attractive interactions between the membrane particles vanish. Consequently, the membrane is split up and remains permanently destroyed, or at least until other mechanisms help the membrane to regenerate. Without the cutoff, the

membrane because of the long-ranged forces always heals after a penetration event.

IV. ANALYTICAL THEORY

To proceed analytically, we restrict ourselves to the small-deformation regime. Then, we linearize the dynamical equations and solve for the membrane displacement and dipole orientation fields.
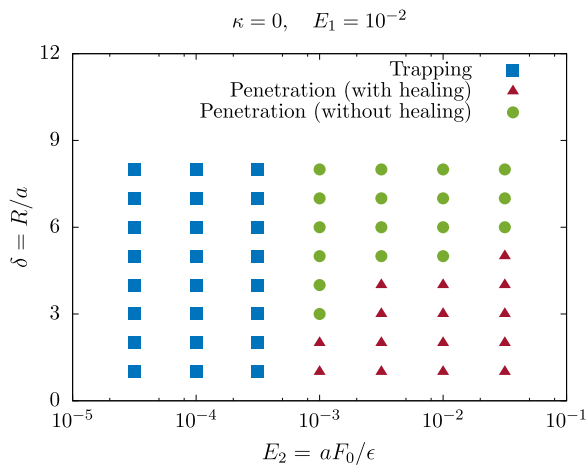
FIG. 4. State diagram of trapping and penetration in the parameter space of size ratio δ and reduced activity E_2, while keeping the reduced stiffness $\kappa = 0$ and the reduced dipole strength $E_1 = 10^{-2}$. Here, we have examined membranes consisting of $N = 20$ dipolar particles. Symbols represent the final dynamical state obtained from numerical integration of Eqs. (5)–(11).

A. Evolution of the membrane particles

In the deformed configuration, the position vector of each dipolar particle in the laboratory frame of reference can be written as $\boldsymbol{r}_i = (d_i + u_i)\hat{\boldsymbol{e}}_x + \rho_i\hat{\boldsymbol{e}}_y$, wherein $d_i = h(i - N/2)$, $i = 1, \ldots, N$, represents the equilibrium x positions of the particles in the initial configuration. Without loss of generality, we consider here only even numbers of N. In addition, u_i and ρ_i denote the membrane displacements along the x and y directions, respectively.

We assume that the active particle has a radius comparable to that of the membrane particles. For the dipolar particles that are not at the chain ends, i.e., for $i = 2, \ldots, N - 1$, the projection of the dynamic equations governing the translational motion of the ith sphere, given by Eq. (8), can be presented in a linearized form as

$$\frac{1}{A}\frac{du_i}{dt} = \frac{72\epsilon\mu}{Ah^2}\left((u_{i+1} - u_i)N_{i,i+1} - (u_i - u_{i-1})N_{i,i-1}\right)$$
$$+ 2(\kappa - 1)\frac{u_{i+1} - 2u_i + u_{i-1}}{h^2} - \frac{\mu F_{\|i}}{A}, \quad (17a)$$

$$\frac{1}{A}\frac{d\rho_i}{dt} = \frac{\rho_{i+1} - 2\rho_i + \rho_{i-1}}{h^2} - \frac{\phi_{i+1} - \phi_{i-1}}{4h} + \frac{\mu F_{\perp i}}{A}, \quad (17b)$$

where we have defined $A := 3\mu_0 m^2\mu/(\pi h^3)$, a parameter that has the dimension of a diffusion coefficient. We assume that $r_{i,i\pm1} < \ell$ always holds in the small-deformation regime considered here. Moreover, $F_{\|i} = F_i \sin\alpha$ and $F_{\perp i} = F_i \cos\alpha$, where $F_i = F(\delta_{i,N/2} + \delta_{i,N/2+1})$ is the magnitude of the force acting on the two central particles due to the steric interactions with the active particle. Thus, $F_i = F$ if $i \in \{N/2, N/2 + 1\}$ and $F_i = 0$ otherwise. This implies that the active particle is exactly positioned between the central two beads of the membrane. We have also explored the situation, where N is an odd number, in

which the external force is only exerted to the center particle and have found quantitatively similar results. Continuing, α is the angle formed by the y axis and the line connecting the center of the self-driven particle to that of the closest membrane particle (see Fig. 1). This angle is defined as negative for clockwise rotation from the y axis. Notably, the dipolar interactions manifest themselves in both the longitudinal and transverse force balance equations, whereas the steric and elastic interactions are (at linear order) only involved in the longitudinal force balance equation. This behavior resembles that of elastic membranes, where stretching and bending effects are predominately pronounced along the tangential and normal traction jumps, respectively.[134–138] Therefore, our self-assembled chains can be used as a minimal model membrane with effective stretching and bending moduli, in analogy to purely elastic membranes with stretching and bending deformation modes.

Similarly, we proceed with the torque balance given by Eq. (11), and derive an approximate equation for the rotational motion of the membrane particles. Upon linearization, we obtain

$$\frac{d\phi_i}{dt} = \frac{B}{2}\left(\frac{\rho_{i+1} - \rho_{i-1}}{h} - \frac{\phi_{i+1} + \phi_{i-1} + 4\phi_i}{3}\right), \quad (18)$$

where we have defined a parameter $B := 3A/(8a^2)$ with the dimension of inverse time. We also used the fact that the translational and rotational mobilities of a sphere are related via $\gamma/\mu = 3/(4a^2)$.

The two particles located at the membrane extremities remain fixed in space (zero displacement) and are not subject to any dipolar torques. The latter could be achieved, for instance, if for the two particles at the ends of the membrane the dipole moment can freely rotate inside the particle, relatively to the particle frame. Therefore, Eqs. (17) and (18) are subject to the boundary conditions

$$u_i = \rho_i = 0 \quad \text{for} \ \ i \in \{1, N\}, \quad (19a)$$

$$\phi_2 + 2\phi_1 - 3\frac{\rho_2}{h} = 0, \quad (19b)$$

$$\phi_{N-1} + 2\phi_N + 3\frac{\rho_{N-1}}{h} = 0. \quad (19c)$$

B. Evolution of the active particle

The active particle is subject to the constant force $\mathbf{F}_0$ acting along the y direction in addition to the resistive forces due to the steric interactions with the two central particles. Denoting by $\mu_P = 1/(6\pi\eta R)$ the translational mobility function of the self-driven particle, the governing equation for the translational motion along the y direction reads

$$\frac{1}{\mu_P}\frac{dy_P}{dt} = F_0 - 2F\cos\alpha. \quad (20)$$

For future reference, we define r as the steady center-to-center distance separating the self-driven particle from the central particles in the trapping state. For an interparticle distance $r \lesssim r_C$, the magnitude of the WCA force acting on a

central particle can, to leading order, be approximated by

$$F = \frac{36 \cdot 2^{2/3}\epsilon}{\sigma}\left(2^{1/6} - \frac{r}{\sigma}\right), \tag{21}$$

where $\sigma = a + R$.

Inserting the latter equation into Eq. (20) and setting the left-hand side to zero, the steady-state distance separating the self-driven particle from the central particles is given by

$$r = \frac{h}{2}\left(1 + \frac{R}{a}\right)\left(1 - \frac{E_2}{288}\left(1 + \frac{R}{a}\right)\frac{h}{a\cos\alpha}\right), \tag{22}$$

where we have used the constraint that $h/a = 2^{7/6}$.

Equations (17) and (18) form $3(N-2)$ ordinary differential equations in time for the unknown displacement and orientation fields. These equations are subject to the six boundary conditions given by Eqs. (19) in addition to the initial conditions of vanishing displacement and orientation fields. In the steady state, the problem reduces to finding the solution of a set of recurrence equations relating the positions and orientations of adjacent spheres. In Sec. V, we present an analytical solution of the resulting recurrence problem. In addition, we show that the underlying equations for the motion of the membrane particles can conveniently be presented in the continuous limit using partial differential equations that describe the temporal and spatial evolution of the membrane displacement and dipole orientation.

V. SOLUTION FOR THE TRAPPING STATE

A. Steady solution of the recurrence problem

For $E_2 \ll 1$, it follows from Eq. (22) that $r \sim h(1 + \delta)/2$, where again $\delta = R/a$. Assuming that $|u_i| \ll h$, for $i = 1, \ldots, N$, yields $\sin\alpha \simeq h/(2r)$. As a result, $\alpha \simeq \arcsin(1/(1 + \delta))$.

Due to the symmetry of the problem with respect to the membrane center, it is sufficient to solve the recurrence problem for $i \in \{1, \ldots, M\}$, where $M := N/2$. In the steady state, it follows readily from the force balance Eq. (20) that $F = F_0/(2\cos\alpha)$, where $\cos\alpha \simeq \left(1 - 1/(1+\delta)^2\right)^{1/2}$.

1. Longitudinal displacement

The mutual distance between adjacent particles in the trapping state is significantly larger than the cutoff distance. Therefore, the steric interactions between membrane particles vanish, and only the elastic and dipolar interactions are relevant.

Assuming that $\kappa \neq 1$, Eq. (17a) that governs the final steady-state membrane displacement along the x direction, for $1 < i < M$, can be written as

$$u_{i+1} - 2u_i + u_{i-1} = 0. \tag{23}$$

The latter expression is subject to the boundary condition $u_{M-1} - 3u_M = Kh$, which follows from setting $i = M$ in Eq. (17a) and using the fact that $u_{M+1} = -u_M$ as required by

symmetry considerations. Here, we have defined for convenience the dimensionless number

$$K = \frac{P_0}{4(\kappa - 1)(1 + \delta)}, \tag{24}$$

where we have used the approximation $\sin\alpha \simeq 1/(1 + \delta)$. The solution of the resulting linear homogeneous second-order recurrence problem satisfying the zero-displacement boundary condition $u_1 = 0$ is given by

$$\frac{u_i}{h} = -\frac{i-1}{N-1}K. \tag{25}$$

The maximum displacement occurs for $i = M$ and amounts to $u_M = -(M-1)Kh/(2M-1)$.

For $\kappa = 1$, the dipolar forces are balanced by the elastic forces. Consequently, the membrane to linear order primarily undergoes motion along the transverse direction.

We further note that for $\kappa \leq 1$ the elastic forces cannot stabilize the system as the dipolar attraction overwhelms the elastic repulsion. Since its ends are fixed, the membrane would tear itself apart. The steric repulsions in this situation prevent the collapse of the system.

2. Transverse displacement and dipole orientation

We next consider the displacement field induced along the transverse direction and examine the rotation of the dipoles. For $1 < i < M$, Eqs. (17b) and (18) are written in the steady trapping state as

$$\frac{1}{h}(\rho_{i+1} - 2\rho_i + \rho_{i-1}) - \frac{1}{4}(\phi_{i+1} - \phi_{i-1}) = 0, \tag{26a}$$

$$\frac{1}{h}(\rho_{i+1} - \rho_{i-1}) - \frac{1}{3}(\phi_{i+1} + 4\phi_i + \phi_{i-1}) = 0. \tag{26b}$$

For the solution of the coupled recurrence relations at hand, it is convenient to rearrange the equations in such a way as to decouple the transverse displacement from the dipole orientation. To this end, we define the displacement gradient as $D_i = (\rho_i - \rho_{i-1})/h$. Accordingly, Eqs. (26) can be rewritten as

$$D_{i+1} - D_i = \frac{1}{4}(\phi_{i+1} - \phi_{i-1}), \tag{27a}$$

$$D_{i+1} + D_i = \frac{1}{3}(\phi_{i+1} + 4\phi_i + \phi_{i-1}). \tag{27b}$$

Then, Eqs. (27) can be rearranged to obtain

$$D_i = \frac{2}{3}\phi_{i-1} + \frac{7\phi_i + \phi_{i-2}}{24} = \frac{2}{3}\phi_i + \frac{7\phi_{i-1} + \phi_{i+1}}{24}. \tag{28}$$

The latter equation can further be rearranged to obtain the following recurrence relation for the orientation field:

$$\phi_{i+1} - \phi_{i-2} + 9(\phi_i - \phi_{i-1}) = 0. \tag{29}$$

In order to solve the resulting linear homogeneous third-order recurrence problem and find the general term of ϕ_i, we use the classical approach based on the *distinct roots theorem*.[139] Correspondingly, we search for solutions of the recurrence relation in the form of $\phi_i = c/p^i$. Substituting into

Eq. (29) yields the characteristic equation of the recurrence problem,

$$p^3 + 9p^2 - 9p - 1 = 0, \qquad (30)$$

the solutions of which, often called the characteristic roots of the recurrence relation, are $p = 1$ and $p_\pm := -5 \pm 2\sqrt{6}$. Then, the general solution for the orientation field is given by

$$\phi_i = C + C_- p_-^i + C_+ p_+^i, \qquad (31)$$

where the constants $C_\pm$ and C are to be determined from the boundary conditions. We note that p_+ and p_- are the multiplicative inverse of each other, i.e., $p_+ p_- = 1$.

Upon substitution of the expression of the orientation field given by Eq. (31) into Eq. (28), the general solution for the displacement gradient is obtained as

$$D_i = C + C_-\left(-1 + \tfrac{\sqrt{6}}{2}\right)p_-^i + C_+\left(-1 - \tfrac{\sqrt{6}}{2}\right)p_+^i. \qquad (32)$$

For the determination of the three unknown coefficients C and $C_\pm$, we make use of the boundary conditions,

$$3D_2 - (\phi_2 + 2\phi_1) = 0, \qquad (33a)$$

$$D_M - \tfrac{1}{4}(\phi_M + \phi_{M-1}) = \tfrac{P_0}{2}, \qquad (33b)$$

$$D_M - \phi_M - \tfrac{\phi_{M-1}}{3} = 0, \qquad (33c)$$

after noting that $\rho_{M+1} = \rho_M$ and $\phi_{M+1} = -\phi_M$. Here, $P_0 = \mu F_0 h / A$ is the dimensionless parameter defined earlier in Eq. (15).

Next, from Eqs. (31) to (33), the unknown coefficients are determined as

$$C = -W\left(12Q_{M-1} + 117Q_M + \sqrt{6}(5S_{M-1} + 48S_M)\right),$$
$$C_\pm = W\left(\pm 12 + 5\sqrt{6}\right),$$

where we have defined

$$S_i = p_+^i + p_-^i, \qquad Q_i = p_+^i - p_-^i. \qquad (34)$$

Moreover, $W = P_0 / \left(3Q_M + \sqrt{6}S_M\right)$.

The transverse displacement field of the ith membrane particle can then be calculated from the displacement gradient as

$$\rho_i = h \sum_{j=2}^{i} D_j, \qquad (35)$$

which, using $\rho_1 = 0$, reads

$$\frac{\rho_i}{h} = (i-1)C + C_-\left(-1 + \tfrac{5\sqrt{6}}{12}\right)\left(49 + 20\sqrt{6} - p_-^{i+1}\right)$$
$$+ C_+\left(1 + \tfrac{5\sqrt{6}}{12}\right)\left(-49 + 20\sqrt{6} + p_+^{i+1}\right). \qquad (36)$$

In the limit of $M \to \infty$ (and thus $h \to 0$ for fixed L), we get $C = P_0$ and $C_- = C_+ = 0$. Defining a continuum variable as $x/L = ((i-1)/(M-1) - 1)/2$ for $1 \le i \le M$ such that $x/L \in [-1/2, 0)$, Eq. (36) can be written in the continuum limit, for x notably smaller than zero, as

$$\lim_{M\to\infty} \phi(x) = P_0, \qquad (37a)$$

$$\lim_{M\to\infty} \rho(x) = P_0\left(\tfrac{L}{2} + x\right). \qquad (37b)$$

It is worth mentioning that our approximation is valid in the small deformation regime for which $P_0 \ll 1$. From parity considerations, consequently $\phi(-x) = -\phi(x)$ and $\rho(-x) = \rho(x)$. Thus, the transverse displacement reaches its maximum value at the membrane center, for $x = 0$.

In the following, we will approach the problem differently by utilizing a continuum description of the governing equations to yield analytical expressions for the membrane deformation not only in the steady state but also in the transient state.

B. Continuum description

In order to obtain a continuum description of the membrane deformation and dipole orientations, we present the transverse displacement field in the form $\rho_{i+s} = \exp(shD)\rho(x)$, and analogously for u_{i+s} and ϕ_{i+s}, wherein s is a relative integer and $D := \partial/\partial x$ denotes the differential operator with respect to the spatial coordinate. Expanding the exponential argument in powers of shD, we obtain for ρ_{i+s} up to second order[140]

$$\rho_{i+s} = \left(1 + sh\frac{\partial}{\partial x} + \frac{(sh)^2}{2}\frac{\partial^2}{\partial x^2} + \cdots\right)\rho(x), \qquad (38)$$

and analogously expressions for u_{i+s} and ϕ_{i+s}.

Using this representation, Eqs. (17) can be written in the continuum limit as

$$u_{,t} = 2A(\kappa - 1)u_{,xx}, \qquad (39a)$$

$$\rho_{,t} = A\left(\rho_{,xx} - \frac{\phi_{,x}}{2}\right) + \mu\left(F_0 - \frac{y_{P,t}}{\mu_P}\right)h\,\delta(x), \qquad (39b)$$

for $-L/2 \le x \le L/2$. Here, commas in the subscripts denote partial derivative with respect to the arguments listed in the subscripts. We have neglected the steric interactions along the longitudinal direction as they usually have a vanishing contribution to the force balance in the trapping state, during which the membrane is stretched. In addition, the discrete force $F_i = F(\delta_{i,M} + \delta_{i,M+1})$ has now been transformed into a point force $2Fh\,\delta(x)$ oriented along the y direction, where the prefactor h has been introduced so as to ensure the right physical dimension. Accordingly, $\alpha \to 0$ holds in the continuum limit since $a \to 0$ leads to $\delta \to \infty$ for R remaining finite. Thus the longitudinal component of the force $F_\parallel$ vanishes.

Similarly, the continuum version of the equation governing the orientation dynamics of the dipoles, given in a discrete form by Eq. (18), reads

$$\phi_{,t} = B(\rho_{,x} - \phi). \qquad (40)$$

Equations (39) and (40) are subject to the initial conditions at $t = 0$ of vanishing displacement and orientation, in addition to the boundary conditions of zero displacement and torque at $x = \pm L/2$. It is worth mentioning that A and B are considered

here as constant membrane properties and are therefore not affected by the limit $h \to 0$.

1. Steady state

We first look for analytical solutions of the continuum model equations in the steady state of motion. It follows from Eq. (39a) that the steady longitudinal displacement in the trapping state satisfies $u_{,xx} = 0$. Since $u(x = 0) = 0$, as required by symmetry considerations, the longitudinal displacement necessarily vanishes upon application of the boundary conditions. Therefore, the membrane particles only displace along the y direction in the considered continuum limit.

As for the transverse displacement, Eq. (39b) simplifies in the steady state to

$$\rho_{,xx} - \frac{\phi_{,x}}{2} + P_0\, \delta(x) = 0, \tag{41}$$

while Eq. (40) leads to $\phi = \rho_{,x}$. As a result, the steady orientation of the dipoles is solely given by the displacement gradient. The present situation is analogous to that known in the context of Kirchhoff–Love theory of elastic beams or plates.[141] Thus, the transverse displacement of the continuous membrane is governed by the following second-order differential equation:

$$\rho_{,xx} + 2P_0\, \delta(x) = 0, \tag{42}$$

the solution of which (that satisfies the boundary conditions) is given by

$$\rho(x) = P_0\left(\frac{L}{2} - |x|\right), \tag{43a}$$

$$\phi(x) = -P_0\, \text{sgn}(x), \tag{43b}$$

where $\text{sgn}(x) \coloneqq x/|x|$ denotes the sign function. These results are in full agreement with Eqs. (37) that have been obtained for $x < 0$ by taking the corresponding continuum limit in the discrete description.

The membrane undergoes a maximum deformation at its center, which, for $h = L/N$ and $h/a = 2^{7/6}$, is given by

$$\frac{\rho_{\text{Max}}}{L} = \frac{P_0}{2} = 4\pi c\, \frac{a^4 F_0}{\mu_0 m^2}, \tag{44}$$

where $c = 2^{5/3}/3 \approx 1.06$ is a numerical prefactor. The latter result indicates that the maximum deflection of the membrane scales linearly with the magnitude of the active force but does not depend on the nature of the steric interactions causing the membrane to deform.

In Fig. 5, we present the steady-state profiles of (a) the transverse displacement $\rho(x)$ and (b) the orientation $\phi(x)$ for various values of E_2, while keeping the other parameters constant at $E_1 = 1$ and $N = 20$. Here, the numerical solutions of the nonlinear equations are indicated by circles, and the results of the corresponding recurrence solution of the linear discrete problem–closely matching the numerical solution– are denoted by squares. Solid lines present the continuum solutions for the same set of parameters.
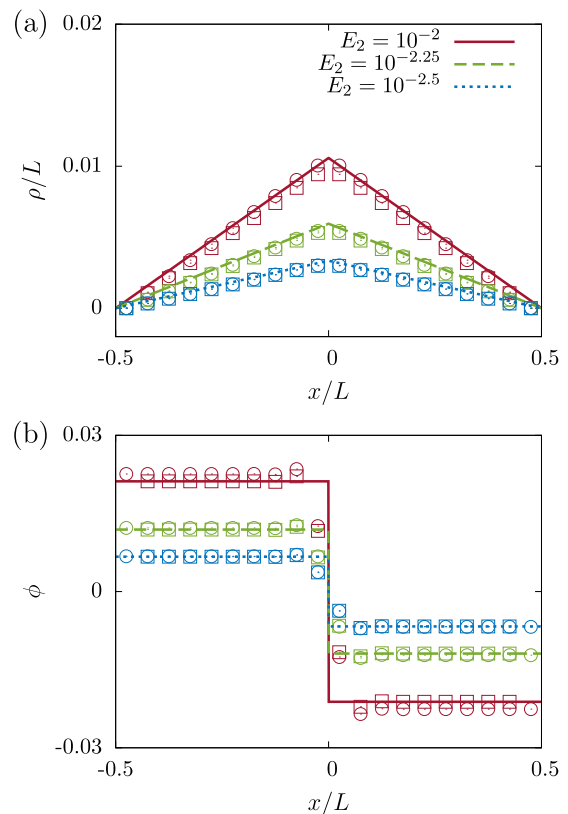
FIG. 5. Steady-state solutions in the trapping state. (a) Scaled membrane deformation ρ/L and (b) local membrane orientation ϕ as functions of x (the self-driven particle is located at $x = 0$), both for systems with $E_1 = 1$, $N = 20$, and varying values of E_2. Circles indicate the results of numerical simulations obtained by solving the nonlinear dynamical equations, squares denote the solutions of the recurrence problem given by Eqs. (31) and (36), and solid lines are the analytical predictions described by Eqs. (43) obtained from a continuum formulation. All these approaches lead to triangular profiles for $\rho(x)$ and square-like ones for $\phi(x)$, showing strong quantitative agreement without the introduction of any fitting parameters.

While the continuum description always leads to ideal triangular and square profiles for $\rho(x)$ and $\phi(x)$, respectively, the numerical solution of the nonlinear problem shows deviations from these shapes. The differences are most probably due to the finite size of the active particle which has not been taken into account in the present continuum description. Finally, we remark that even though no fitting parameters have been introduced, the results still closely match each other, reinforcing the applicability of our approximate analytical approach to predict the shape of our minimal membrane model under the influence of a localized destroying force.

2. Transient behavior

Having presented analytical solutions of the continuum equations of motion in the steady state, assessed the appropriateness and judged the accuracy of our linearized

analytical theory, we next address the membrane deformation and dipole orientation in the transient regime. The solution to this mathematical problem can be obtained by *finite* Fourier transforms in space of the governing equations and solving the resulting ordinary differential equations in time.

For this purpose, we define the basis functions

$$c_q(x) = \cos(H_q x), \qquad s_q(x) = \sin(H_q x), \qquad (45)$$

where $H_q = (2q - 1)\pi/L$ with $q = 1, 2, \ldots$ denoting the variable that sets the coordinates in Fourier space. Then the displacement and orientation fields can be expressed in terms of Fourier series in space as[142]

$$\rho(x, t) = \frac{2}{L} \sum_{q \geq 1} \hat{\rho}(q, t) \, c_q(x), \qquad (46a)$$

$$\phi(x, t) = \frac{2}{L} \sum_{q \geq 1} \hat{\phi}(q, t) \, s_q(x), \qquad (46b)$$

where $\hat{\rho}$ and $\hat{\phi}$ are the Fourier coefficients, defined as

$$\hat{\rho}(q, t) = \int_{-\frac{L}{2}}^{\frac{L}{2}} \rho(x, t) \, c_q(x) \, dx, \qquad (47a)$$

$$\hat{\phi}(q, t) = \int_{-\frac{L}{2}}^{\frac{L}{2}} \phi(x, t) \, s_q(x) \, dx. \qquad (47b)$$

The form of the Fourier representation given by Eqs. (46) follows from the boundary conditions to ensure at any time that $\rho(\pm L/2, t) = 0$ and $\phi_{,x}(\pm L/2, t) = 0$. We note that the basis functions $c_q(x)$ and $s_q(x)$ satisfy the orthogonality relations

$$\int_{-\frac{L}{2}}^{\frac{L}{2}} c_p(x) c_q(x) \, dx = \int_{-\frac{L}{2}}^{\frac{L}{2}} s_p(x) s_q(x) \, dx = \frac{L}{2} \, \delta_{pq}. \qquad (48)$$

Transforming Eqs. (39b) and (40) into spatial Fourier space yields

$$\frac{\hat{\rho}_{,t}}{A} = -H_q\left(H_q\hat{\rho} + \frac{\hat{\phi}}{2}\right) + P_0\left(1 - \frac{y_{P,t}}{v_0}\right), \qquad (49a)$$

$$\frac{\hat{\phi}_{,t}}{B} = -H_q\hat{\rho} - \hat{\phi}, \qquad (49b)$$

where $v_0 = \mu_P F_0$ is the bulk velocity of the active particle.

For a closure of the above set of equations, we require that the instantaneous distance between the self-driven particle and the membrane center remains constant during the system evolution such that $y_{P,t} = \rho_{,t}(x = 0, t)$. However, in order to be able to make analytical progress, we further assume that after a brief transient evolution, $|y_{P,t}| \ll v_0$ holds, and thus the term involving $y_{P,t}$ can be neglected. This is equivalent to assuming that the active particle instantaneously attains its terminal velocity when the interaction with the membrane takes place.

The solution of the system of differential equations given by Eqs. (49) can more easily be obtained using the Laplace transform technique.[143] In the following, the Laplace-transformed function pairs are distinguished only by their argument while the hat is reserved to denote the

spatial Fourier transforms. By employing the initial conditions $\hat{\rho}(q, t = 0) = \hat{\phi}(q, t = 0) = 0$, we obtain

$$\frac{s}{A} \, \hat{\rho}(q, s) = -H_q\left(H_q\hat{\rho}(q, s) + \frac{\hat{\phi}(q, s)}{2}\right) + \frac{P_0}{s}, \qquad (50a)$$

$$\frac{s}{B} \, \hat{\phi}(q, s) = -H_q\hat{\rho}(q, s) - \hat{\phi}(q, s). \qquad (50b)$$

Solving these equations for $\hat{\rho}(q, s)$ and $\hat{\phi}(q, s)$ yields

$$\hat{\rho}(q, s) = \frac{2A(B + s)P_0}{Q}, \qquad (51a)$$

$$\hat{\phi}(q, s) = -\frac{2H_qABP_0}{Q}, \qquad (51b)$$

where the denominator is given by

$$Q = s\left(2s^2 + 2(B + AH_q^2)s + ABH_q^2\right).$$

The inverse Laplace transform can readily be obtained from the standard approach of partial fraction decomposition and using tables of Laplace transforms, which yields

$$\hat{\rho}(q, t) = \frac{2P_0}{H_q^2}\left(1 - e^{-\beta t}\left(\cosh(\tau t) + \frac{B}{2\tau} \, \sinh(\tau t)\right)\right),$$

$$\hat{\phi}(q, t) = -\frac{2P_0}{H_q}\left(1 - e^{-\beta t}\left(\cosh(\tau t) + \frac{\beta}{\tau} \, \sinh(\tau t)\right)\right),$$

where we have defined the parameters τ and β, with inverse time dimension, as

$$\tau = \frac{1}{2}\sqrt{B^2 + A^2H_q^4}, \qquad \beta = \frac{1}{2}\left(B + AH_q^2\right). \qquad (52)$$

A typical transient behavior is shown in Fig. 6 presenting (a) the membrane transverse displacement $\rho(x, t)$ and (b) the dipole orientation $\phi(x, t)$ at various times t using the parameters $E_1 = 1$, $E_2 = 10^{-2}$, and $N = 20$. Here, symbols indicate the numerical solutions for a discrete membrane and solid lines represent the analytical solutions of the continuum theory outlined above. Again, without fitting parameters, there is strong qualitative and quantitative agreement between both approaches.

The transverse displacement profile features at early times a small central dent, which then more and more expands as time evolves. This leads to a significant kink at the center and, finally, to the triangular shape in the steady state. At all times, the symmetry $\rho(-x, t) = \rho(x, t)$ is fulfilled. Similarly, for the dipole orientation, smooth transitions take place from a small "orientation jump" in the center and vanishing initial orientations elsewhere to a full-chain square-like profile in the steady state. The discrete case features a significantly less pronounced change in orientation for the two central spheres at all times.

Finally, we address the transient behavior in the particular situation of fast orientational relaxation, for which $B \gg Aq^2$. Setting $\phi_{,t} = 0$ in Eq. (40) yields
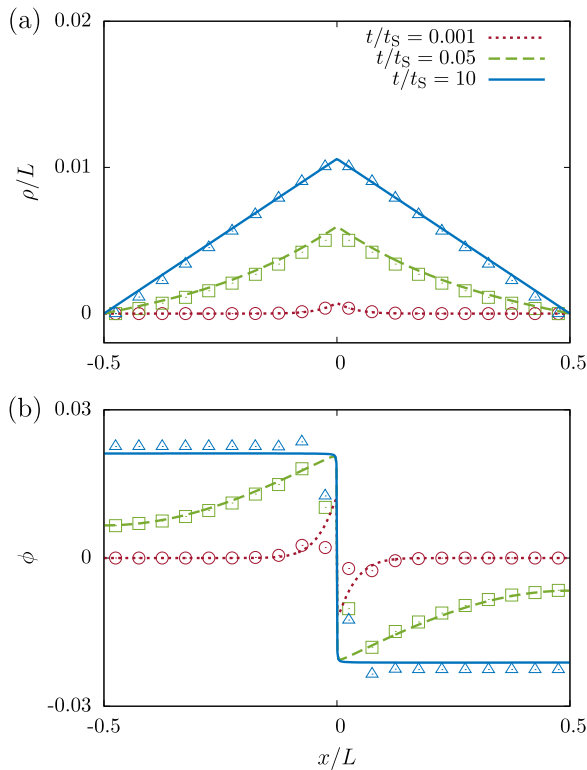
FIG. 6. Dynamic solutions for the trapping scenario. (a) Scaled transient membrane deformation profile $\rho(x, t)/L$ and (b) membrane orientation profile $\phi(x, t)$ calculated at times $t/t_S = 0.001, 0.05, 10$, where $t_S = \eta L^3/\epsilon$ for $N = 20$, $E_1 = 1$, and $E_2 = 10^{-2}$. Here, symbols are numerical simulation results and solid lines give the corresponding analytical results according to Eqs. (46). Both approaches show qualitative and quantitative agreement in their description of the transition from the small central perturbations at early times to the steady state for $t \to \infty$ (see also Fig. 5 for a detailed display of the latter).

$$\phi = \rho_{,x}. \tag{53}$$

Accordingly, the dipole orientation follows instantaneously the slope of the membrane. Inserting Eq. (53) into Eq. (39b) yields

$$\rho_{,t} = \frac{A}{2}\rho_{,xx} + \mu h F_0 \,\delta(x), \tag{54}$$

where $y_{P,t}$ has been neglected along the same lines as discussed above.

Equation (54) has the form of a diffusion equation with a point source localized in space, subject to the initial condition $\rho(x, t = 0) = 0$, in addition to the Dirichlet-type boundary conditions $\rho(x = \pm L/2, t) = 0$. The solution of this equation has been obtained by Sommerfeld[144] and is expressed as

$$\rho(x, t) = \frac{A P_0}{2L} \int_0^t \left(\vartheta\left(\frac{x}{2L}, t'\right) - \vartheta\left(\frac{x+L}{2L}, t'\right) \right) dt', \tag{55}$$

with Jacobi theta functions[145]

$$\vartheta(\xi, t) = 1 + 2 \sum_{n=1}^{\infty} e^{-\delta_n t} \cos(2n\pi\xi), \tag{56}$$

where we have defined

$$\delta_n = \frac{n^2\pi^2 A}{2L^2}. \tag{57}$$

This leads to the scaled displacement

$$\frac{\rho(x, t)}{L} = \frac{4P_0}{\pi^2} \sum_{n=1}^{\infty} \frac{1 - e^{-\delta_{2n-1}t}}{(2n-1)^2} \cos\left((2n-1)\frac{\pi x}{L}\right), \tag{58}$$

which reproduces the steady-state solution given by Eq. (36) as shown below. In particular, the long-time behavior is dominated by the first term ($n = 1$), which approaches the limit exponentially with a characteristic decay time $2L^2/(\pi^2 A)$. Additionally, the orientation follows forthwith from Eq. (53) as

$$\phi(x, t) = -\frac{4P_0}{\pi} \sum_{n=1}^{\infty} \frac{1 - e^{-\delta_{2n-1}t}}{2n-1} \sin\left((2n-1)\frac{\pi x}{L}\right). \tag{59}$$

In the limit $t \to \infty$, we obtain

$$\lim_{t\to\infty} \frac{\rho(x, t)}{L} = \frac{4P_0}{\pi^2} \sum_{n=1}^{\infty} \frac{\cos\left((2n-1)\frac{\pi x}{L}\right)}{(2n-1)^2}, \tag{60a}$$

$$\lim_{t\to\infty} \phi(x, t) = -\frac{4P_0}{\pi} \sum_{n=1}^{\infty} \frac{\sin\left((2n-1)\frac{\pi x}{L}\right)}{2n-1}, \tag{60b}$$

which correspond, respectively, to the Fourier series representation of the triangle and square wave functions of frequency $2\pi/L$. The maximum membrane displacement is calculated as

$$\lim_{t\to\infty} \frac{\rho(0, t)}{L} = \frac{4P_0}{\pi^2} \sum_{n=1}^{\infty} \frac{1}{(2n-1)^2} = \frac{P_0}{2}, \tag{61}$$

in agreement with the result obtained earlier from the steady differential equations, as given by Eq. (44).

VI. CONCLUSIONS

In this article, we explored the interactions between an active particle and a minimal model membrane. Since we concentrate on a two-dimensional setup, our results could, for instance, in experiments be readily compared with the behavior of a self-driven particle on a substrate, colliding with a straightened chain of mutually attractive dipolar spheres. We demonstrated that the particle may either get trapped by the membrane or penetrate through it, where the membrane can either be permanently damaged or recover by self-healing. State diagrams are presented that carefully map out which state occurs as a function of only a few generic parameters: membrane elasticity, bending stiffness, strength and size of the active particle. Our analytical theory further predicts the shape and the dynamics of the membrane, in close quantitative agreement with our numerical simulations. Our results suggest that the microscopic details of the interactions among membrane components (particles) are largely insignificant to the overall behavior of the membrane. Thus, our results

might be broadly applicable to describe the experiments of micro-swimmers interacting with membranes, such as synthetic microbots colliding with a lipid bilayer or microbes with a membrane synthesized from dipolar microparticles. In this context, it would be interesting to extend our model to account for Brownian noise acting on the membrane and the self-driven particle as well. This might, for instance, support the membrane in healing after being destroyed by the penetrating active particle.

ACKNOWLEDGMENTS

REFERENCES

[1] K. T. Kaljot, R. D. Shaw, D. H. Rubin, and H. B. Greenberg, "Infectious rotavirus enters cells by direct cell membrane penetration, not by endocytosis," J. Virol. **62**, 1136–1144 (1988), available at https://jvi.asm.org/content/62/4/1136.

[2] H. Lodish, A. Berk, S. L. Zipursky, P. Matsudaira, D. Baltimore, J. Darnell *et al.*, *Molecular Cell Biology* (W. H. Freeman, New York, 1995), Vol. 3.

[3] G. Seisenberger, M. U. Ried, T. Endreß, H. Büning, M. Hallek, and C. Bräuchle, "Real-time single-molecule imaging of the infection pathway of an adeno-associated virus," Science **294**, 1929–1932 (2001).

[4] K. Saar, M. Lindgren, M. Hansen, E. Eiríksdóttir, Y. Jiang, K. Rosenthal-Aizman, M. Sassian, and Ü. Langel, "Cell-penetrating peptides: A comparative membrane toxicity study," Anal. Biochem. **345**, 55–65 (2005).

[5] G. Karp, *Cell and Molecular Biology: Concepts and Experiments* (Wiley, Hoboken, NJ, 2008).

[6] Y. Li, H. Yuan, A. von dem Bussche, M. Creighton, R. H. Hurt, A. B. Kane, and H. Gao, "Graphene microsheets enter cells through spontaneous membrane penetration at edge asperities and corner sites," Proc. Natl. Acad. Sci. U. S. A. **110**, 12295–12300 (2013).

[7] A. R. Liboff, "Magnetic correlates in electromagnetic consciousness," Electromagn. Biol. Med. **35**, 228–236 (2016).

[8] Y. Xia, "Nanomaterials at work in biomedical research," Nat. Mater. **7**, 758 (2008).

[9] D. K. Kirui, D. A. Rey, and C. A. Batt, "Gold hybrid nanoparticles for targeted phototherapy and cancer imaging," Nanotechnology **21**, 105105 (2010).

[10] J. S. Suk, Q. Xu, N. Kim, J. Hanes, and L. M. Ensign, "PEGylation as a strategy for improving nanoparticle-based drug and gene delivery," Adv. Drug Delivery Rev. **99**, 28–51 (2016).

[11] C. Lanvers-Kaminsky, A. am Zehnhoff-Dinnesen, R. Parfitt, and G. Ciarimboli, "Drug-induced ototoxicity: Mechanisms, pharmacogenetics, and protective strategies," Clin. Pharmacol. Ther. **101**, 491–500 (2017).

[12] K. B. Jirage, J. C. Hulteen, and C. R. Martin, "Nanotubule-based molecular-filtration membranes," Science **278**, 655–658 (1997).

[13] S. Y. Yang, I. Ryu, H. Y. Kim, J. K. Kim, S. K. Jang, and T. P. Russell, "Nanoporous membranes with ultrahigh selectivity and flux for the filtration of viruses," Adv. Mater. **18**, 709–712 (2006).

[14] A. Kalra, S. Garde, and G. Hummer, "Osmotic water transport through carbon nanotube membranes," Proc. Natl. Acad. Sci. U. S. A. **100**, 10175–10180 (2003).

[15] P. Nelson, *Biological Physics* (W. H. Freeman, New York, 2004).

[16] H. Nikaido and M. H. Saier, "Transport proteins in bacteria: Common themes in their design," Science **258**, 936–942 (1992).

[17] M. Palacín, R. Estévez, J. Bertran, and A. Zorzano, "Molecular biology of mammalian plasma membrane amino acid transporters," Physiol. Rev. **78**, 969–1054 (1998).

[18] E. R. Kandel, J. H. Schwartz, T. M. Jessell, D. of Biochemistry, M. B. T. Jessell, S. Siegelbaum, and A. Hudspeth, *Principles of Neural Science* (McGraw-Hill, New York, 2000), Vol. 4.

[19] I. A. Simpson, A. Carruthers, and S. J. Vannucci, "Supply and demand in cerebral energy metabolism: The role of nutrient transporters," J. Cereb. Blood Flow Metab. **27**, 1766–1791 (2007).

[20] M. Yu, L. Xu, F. Tian, Q. Su, N. Zheng, Y. Yang, J. Wang, A. Wang, C. Zhu, S. Guo *et al.*, "Rapid transport of deformation-tuned nanoparticles across biological hydrogels and cellular barriers," Nat. Commun. **9**, 2607 (2018).

[21] A. J. T. M. Mathijssen, R. Jeanneret, and M. Polin, "Universal entrainment mechanism controls contact times with motile cells," Phys. Rev. Fluids **3**, 033103 (2018).

[22] C. Gräfe, I. Slabu, F. Wiekhorst, C. Bergemann, F. von Eggeling, A. Hochhaus, L. Trahms, and J. Clement, "Magnetic particle spectroscopy allows precise quantification of nanoparticles after passage through human brain microvascular endothelial cells," Phys. Med. Biol. **61**, 3986 (2016).

[23] F. Schlenk, S. Werner, M. Rabel, F. Jacobs, C. Bergemann, J. H. Clement, and D. Fischer, "Comprehensive analysis of the *in vitro* and ex ovo hemocompatibility of surface engineered iron oxide nanoparticles for biomedical applications," Arch. Toxicol. **91**, 3271–3286 (2017).

[24] E. K. Müller, C. Gräfe, F. Wiekhorst, C. Bergemann, A. Weidner, S. Dutz, and J. H. Clement, "Magnetic nanoparticles interact and pass an *in vitro* co-culture blood-placenta barrier model," Nanomaterials **8**, 108 (2018).

[25] B. D. Chithrani, A. A. Ghazani, and W. C. W. Chan, "Determining the size and shape dependence of gold nanoparticle uptake into mammalian cells," Nano Lett. **6**, 662–668 (2006).

[26] J. Lin, H. Zhang, Z. Chen, and Y. Zheng, "Penetration of lipid membranes by gold nanoparticles: Insights into cellular uptake, cytotoxicity, and their relationship," ACS Nano **4**, 5421–5429 (2010).

[27] K. Yang and Y. Q. Ma, "Computer simulation of the translocation of nanoparticles with different shapes across a lipid bilayer," Nat. Nanotechnol. **5**, 579–583 (2010).

[28] T. Dos Santos, J. Varela, I. Lynch, A. Salvati, and K. A. Dawson, "Quantitative assessment of the comparative nanoparticle-uptake efficiency of a range of cell lines," Small **7**, 3341–3349 (2011).

[29] S. Dasgupta, T. Auth, and G. Gompper, "Shape and orientation matter for the cellular uptake of nonspherical particles," Nano Lett. **14**, 687–693 (2014).

[30] S. Dasgupta, T. Auth, and G. Gompper, "Nano- and microparticles at fluid and biological interfaces," J. Phys.: Condens. Matter **29**, 373003 (2017).

[31] E. Barry and Z. Dogic, "Entropy driven self-assembly of nonamphiphilic colloidal membranes," Proc. Natl. Acad. Sci. U. S. A. **107**, 10348–10353 (2010).

[32] K. Zahn and G. Maret, "Two-dimensional colloidal structures responsive to external fields," Curr. Opin. Colloid Interface Sci. **4**, 60–65 (1999).

[33] M. Mittal and E. M. Furst, "Electric field-directed convective assembly of ellipsoidal colloidal particles to create optically and mechanically anisotropic thin films," Adv. Funct. Mater. **19**, 3271–3278 (2009).

[34] N. Osterman, I. Poberaj, J. Dobnikar, D. Frenkel, P. Ziherl, and D. Babić, "Field-induced self-assembly of suspended colloidal membranes," Phys. Rev. Lett. **103**, 228301 (2009).

[35] E. C. Oğuz, M. Marechal, F. Ramiro-Manzano, I. Rodriguez, R. Messina, F. J. Meseguer, and H. Löwen, "Packing confined hard spheres denser with adaptive prism phases," Phys. Rev. Lett. **109**, 218301 (2012).

[36] J. Dobnikar, A. Snezhko, and A. Yethiraj, "Emergent colloidal dynamics in electromagnetic fields," Soft Matter **9**, 3693–3704 (2013).

[37] I. Williams, E. C. Oğuz, T. Speck, P. Bartlett, H. Löwen, and C. P. Royall, "Transmission of torque at the nanoscale," Nat. Phys. **12**, 98 (2016).

[38] A. Ortiz-Ambriz and P. Tierno, "Engineering of frustration in colloidal artificial ices realized on microfeatured grooved lattices," Nat. Commun. **7**, 10575 (2016).

[39] J. Loehr, A. Ortiz-Ambriz, and P. Tierno, "Defect dynamics in artificial colloidal ice: Real-time observation, manipulation, and logic gate," Phys. Rev. Lett. **117**, 168001 (2016).

[40] P. Tierno, "Geometric frustration of colloidal dimers on a honeycomb magnetic lattice," Phys. Rev. Lett. **116**, 038303 (2016).

[41] W. Shenton, S. A. Davis, and S. Mann, "Directed self-assembly of nanoparticles into macroscopic materials using antibody–antigen recognition," Adv. Mater. **11**, 449–452 (1999).

[42] M. Grzelczak, J. Vermant, E. M. Furst, and L. M. Liz-Marzán, "Directed self-assembly of nanoparticles," ACS Nano **4**, 3591–3605 (2010).

[43] V. Froltsov, R. Blaak, C. Likos, and H. Löwen, "Crystal structures of two-dimensional magnetic colloids in tilted external magnetic fields," Phys. Rev. E **68**, 061406 (2003).

[44] V. Froltsov, C. N. Likos, H. Löwen, C. Eisenmann, U. Gasser, P. Keim, and G. Maret, "Anisotropic mean-square displacements in two-dimensional colloidal crystals of tilted dipoles," Phys. Rev. E **71**, 031404 (2005).

[45] Y. Lin, A. Böker, J. He, K. Sill, H. Xiang, C. Abetz, X. Li, J. Wang, T. Emrick, S. Long et al., "Self-directed self-assembly of nanoparticle/copolymer mixtures," Nature **434**, 55 (2005).

[46] D. Heinrich, A. R. Goñi, T. Osan, L. Cerioni, A. Smessaert, S. H. Klapp, J. Faraudo, D. J. Pusiol, and C. Thomsen, "Effects of magnetic field gradients on the aggregation dynamics of colloidal magnetic nanoparticles," Soft Matter **11**, 7606–7616 (2015).

[47] A. B. Yener and S. H. Klapp, "Self-assembly of three-dimensional ensembles of magnetic particles with laterally shifted dipoles," Soft Matter **12**, 2066–2075 (2016).

[48] S. D. Peroukidis and S. H. L. Klapp, "Orientational order and translational dynamics of magnetic particle assemblies in liquid crystals," Soft Matter **12**, 6841–6850 (2016).

[49] B. Bharti, F. Kogler, C. K. Hall, S. H. Klapp, and O. D. Velev, "Multidirectional colloidal assembly in concurrent electric and magnetic fields," Soft Matter **12**, 7747–7758 (2016).

[50] Q. A. Pankhurst, J. Connolly, S. Jones, and J. Dobson, "Applications of magnetic nanoparticles in biomedicine," J. Phys. D: Appl. Phys. **36**, R167 (2003).

[51] A.-H. Lu, E. L. Salabas, and F. Schüth, "Magnetic nanoparticles: Synthesis, protection, functionalization, and application," Angew. Chem., Int. Ed. **46**, 1222–1244 (2007).

[52] S. Naahidi, M. Jafari, F. Edalat, K. Raymond, A. Khademhosseini, and P. Chen, "Biocompatibility of engineered nanoparticles for drug delivery," J. Controlled Release **166**, 182–194 (2013).

[53] H. Al-Obaidi and A. T. Florence, "Nanoparticle delivery and particle diffusion in confined and complex environments," J. Drug Delivery Sci. Technol. **30**, 266–277 (2015).

[54] J. Liu, T. Wei, J. Zhao, Y. Huang, H. Deng, A. Kumar, C. Wang, Z. Liang, X. Ma, and X.-J. Liang, "Multifunctional aptamer-based nanoparticles for targeted drug delivery to circumvent cancer resistance," Biomaterials **91**, 44–56 (2016).

[55] J. Gao, H. Gu, and B. Xu, "Multifunctional magnetic nanoparticles: Design, synthesis, and biomedical applications," Acc. Chem. Res. **42**, 1097–1107 (2009).

[56] N. Wang, J. Butler, and D. Ingber, "Mechanotransduction across the cell surface and through the cytoskeleton," Science **260**, 1124–1127 (1993).

[57] J. Dobson, "Remote control of cellular behaviour with magnetic nanoparticles," Nat. Nanotechnol. **3**, 139 (2008).

[58] Q. A. Pankhurst, N. T. K. Thanh, S. K. Jones, and J. Dobson, "Progress in applications of magnetic nanoparticles in biomedicine," J. Phys. D: Appl. Phys. **42**, 224001 (2009).

[59] M. Ewerlin, D. Demirbas, F. Brüssing, O. Petracic, A. A. Ünal, S. Valencia, F. Kronast, and H. Zabel, "Magnetic dipole and higher pole interaction on a square lattice," Phys. Rev. Lett. **110**, 177209 (2013).

[60] L. Spiteri and R. Messina, "Columnar aggregation of dipolar chains," Europhys. Lett. **120**, 36001 (2017).

[61] R. Messina, L. A. Khalil, and I. Stanković, "Self-assembly of magnetic balls: From chains to tubes," Phys. Rev. E **89**, 011202 (2014).

[62] R. Messina and I. Stanković, "Assembly of magnetic spheres in strong homogeneous magnetic field," Physica A **466**, 10–20 (2017).

[63] F. Guzmán-Lastra, A. Kaiser, and H. Löwen, "Fission and fusion scenarios for magnetic microswimmer clusters," Nat. Commun. **7**, 13519 (2016).

[64] F. Martinez-Pedrero, A. Ortiz-Ambriz, I. Pagonabarraga, and P. Tierno, "Colloidal microworms propelling via a cooperative hydrodynamic conveyor belt," Phys. Rev. Lett. **115**, 138301 (2015).

[65] A. Kaiser, K. Popowa, and H. Löwen, "Active dipole clusters: From helical motion to fission," Phys. Rev. E **92**, 012301 (2015).

[66] S. Babel, H. Löwen, and A. M. Menzel, "Dynamics of a linear magnetic 'microswimmer molecule'," Europhys. Lett. **113**, 58003 (2016).

[67] A. J. T. M. Mathijssen, A. Doostmohammadi, J. M. Yeomans, and T. N. Shendruk, "Hydrodynamics of microswimmers in films," J. Fluid Mech. **806**, 35–70 (2016).

[68] J. Elgeti, R. G. Winkler, and G. Gompper, "Physics of microswimmers–Single particle motion and collective behavior: A review," Rep. Prog. Phys. **78**, 056601 (2015).

[69] C. Bechinger, R. Di Leonardo, H. Löwen, C. Reichhardt, G. Volpe, and G. Volpe, "Active particles in complex and crowded environments," Rev. Mod. Phys. **88**, 045006 (2016).

[70] J. de Graaf, H. Menke, A. J. T. M. Mathijssen, M. Fabritius, C. Holm, and T. Shendruk, "Lattice-Boltzmann hydrodynamics of anisotropic active matter," J. Chem. Phys. **144**, 134106 (2016).

[71] F. Martinez-Pedrero, E. Navarro-Argemí, A. Ortiz-Ambriz, I. Pagonabarraga, and P. Tierno, "Emergent hydrodynamic bound states between magnetically powered micropropellers," Sci. Adv. **4**, eaap9379 (2018).

[72] A. Daddi-Moussa-Ider, M. Lisicki, C. Hoell, and H. Löwen, "Swimming trajectories of a three-sphere microswimmer near a wall," J. Chem. Phys. **148**, 134904 (2018).

[73] A. Daddi-Moussa-Ider, M. Lisicki, A. J. T. M. Mathijssen, C. Hoell, S. Goh, J. Bławzdziewicz, A. M. Menzel, and H. Löwen, "State diagram of a three-sphere microswimmer in a channel," J. Phys.: Condens. Matter **30**, 254004 (2018).

[74] J. García-Torres, C. Calero, F. Sagués, I. Pagonabarraga, and P. Tierno, "Magnetically tunable bidirectional locomotion of a self-assembled nanorod-sphere propeller," Nat. Commun. **9**, 1663 (2018).

[75] T. Yu, P. Chuphal, S. Thakur, S.-Y. Reigh, D. P. Singh, and P. Fischer, "Chemical micromotors self-assemble and self-propel by spontaneous symmetry breaking," Chem. Commun. **54**, 11933 (2018).

[76] A. J. Mathijssen, F. Guzmán-Lastra, A. Kaiser, and H. Löwen, "Nutrient transport driven by microbial active carpets," Phys. Rev. Lett. **121**, 248101 (2018).

[77] A. Daddi-Moussa-Ider and A. M. Menzel, "Dynamics of a simple model microswimmer in an anisotropic fluid: Implications for alignment behavior and active transport in a nematic liquid crystal," Phys. Rev. Fluids **3**, 094102 (2018).

[78] A. Kaiser, S. Babel, B. ten Hagen, C. von Ferber, and H. Löwen, "How does a flexible chain of active particles swell?," J. Chem. Phys. **142**, 124905 (2015).

[79] R. G. Winkler, J. Elgeti, and G. Gompper, "Active polymers–emergent conformational and dynamical properties: A brief review," J. Phys. Soc. Jpn. **86**, 101014 (2017).

[80] A. Martín-Gómez, G. Gompper, and R. Winkler, "Active brownian filamentous polymers under shear flow," Polymers **10**, 837 (2018).

[81] Ö. Duman, R. E. Isele-Holder, J. Elgeti, and G. Gompper, "Collective dynamics of self-propelled semiflexible filaments," Soft Matter **14**, 4483–4494 (2018).

[82]Y. Peng, H. Zhang, X.-W. Huang, J.-H. Huang, and M.-B. Luo, "Monte Carlo simulation on the dynamics of a semi-flexible polymer in the presence of nanoparticles," Phys. Chem. Chem. Phys. **20**, 26333–26343 (2018).

[83]J. Shin, A. G. Cherstvy, W. K. Kim, and R. Metzler, "Facilitation of polymer looping and giant polymer diffusivity in crowded solutions of active particles," New J. Phys. **17**, 113008 (2015).

[84]B. ten Hagen, S. van Teeffelen, and H. Löwen, "Brownian motion of a self-propelled particle," J. Phys.: Condens. Matter **23**, 194119 (2011).

[85]R. Wittkowski and H. Löwen, "Self-propelled brownian spinning top: Dynamics of a biaxial swimmer at low Reynolds numbers," Phys. Rev. E **85**, 021406 (2012).

[86]A. Kaiser, H. Wensink, and H. Löwen, "How to capture active particles," Phys. Rev. Lett. **108**, 268307 (2012).

[87]H. H. Wensink and H. Löwen, "Emergent states in dense systems of active rods: From swarming to turbulence," J. Phys.: Condens. Matter **24**, 464130 (2012).

[88]F. Kümmel, B. ten Hagen, R. Wittkowski, I. Buttinoni, R. Eichhorn, G. Volpe, H. Löwen, and C. Bechinger, "Circular motion of asymmetric self-propelling particles," Phys. Rev. Lett. **110**, 198302 (2013).

[89]B. ten Hagen, F. Kümmel, R. Wittkowski, D. Takagi, H. Löwen, and C. Bechinger, "Gravitaxis of asymmetric self-propelled colloidal particles," Nat. Commun. **5**, 4829 (2014).

[90]B. ten Hagen, R. Wittkowski, D. Takagi, F. Kümmel, C. Bechinger, and H. Löwen, "Can the self-propulsion of anisotropic microswimmers be described by using forces and torques?," J. Phys.: Condens. Matter **27**, 194110 (2015).

[91]T. Speck and R. L. Jack, "Ideal bulk pressure of active brownian particles," Phys. Rev. E **93**, 062605 (2016).

[92]M. Driscoll and B. Delmotte, "Leveraging collective effects in externally driven colloidal suspensions: Experiments and simulations," Curr. Opin. Colloid Interface Sci. **40**, 42 (2018).

[93]W. Gao, X. Feng, A. Pei, C. R. Kane, R. Tam, C. Hennessy, and J. Wang, "Bioinspired helical microswimmers based on vascular plants," Nano Lett. **14**, 305–310 (2013).

[94]W. Gao and J. Wang, "Synthetic micro/nanomotors in drug delivery," Nanoscale **6**, 10486–10494 (2014).

[95]C. Scholz, M. Engel, and T. Pöschel, "Rotating robots move collectively and self-organize," Nat. Commun. **9**, 931 (2018).

[96]C. Scholz, S. Jahanshahi, A. Ldov, and H. Löwen, "Inertial delay of self-propelled particles," Nat. Commun. **9**, 5156 (2018).

[97]B. J. Nelson, I. K. Kaliakatsos, and J. J. Abbott, "Microrobots for minimally invasive medicine," Annu. Rev. Biomed. Eng. **12**, 55–85 (2010).

[98]W. Xi, A. A. Solovev, A. N. Ananth, D. H. Gracias, S. Sanchez, and O. G. Schmidt, "Rolled-up magnetic microdrillers: Towards remotely controlled minimally invasive surgery," Nanoscale **5**, 1294–1297 (2013).

[99]L. K. Abdelmohsen, F. Peng, Y. Tu, and D. A. Wilson, "Micro-and nanomotors for biomedical applications," J. Mater. Chem. B **2**, 2395–2408 (2014).

[100]J. Wang and W. Gao, "Nano/microscale motors: Biomedical opportunities and challenges," ACS Nano **6**, 5745–5751 (2012).

[101]W. Wang, W. Duan, S. Ahmed, T. E. Mallouk, and A. Sen, "Small power: Autonomous nano- and micromotors propelled by self-generated gradients," Nano Today **8**, 531–554 (2013).

[102]W. F. Paxton, K. C. Kistler, C. C. Olmeda, A. Sen, S. K. St. Angelo, Y. Cao, T. E. Mallouk, P. E. Lammert, and V. H. Crespi, "Catalytic nanomotors: Autonomous movement of striped nanorods," J. Am. Chem. Soc. **126**, 13424–13431 (2004).

[103]W. Wang, S. Li, L. Mair, S. Ahmed, T. J. Huang, and T. E. Mallouk, "Acoustic propulsion of nanorod motors inside living cells," Angew. Chem., Int. Ed. **53**, 3201–3204 (2014).

[104]U. Marini Bettolo Marconi, A. Sarracino, C. Maggi, and A. Puglisi, "Self-propulsion against a moving membrane: Enhanced accumulation and drag force," Phys. Rev. E **96**, 032601 (2017).

[105]G. Junot, G. Briand, R. Ledesma-Alonso, and O. Dauchot, "Active versus passive hard disks against a membrane: Mechanical pressure and instability," Phys. Rev. Lett. **119**, 028002 (2017).

[106]A. F. Demirörs, J. C. Stiefelhagen, T. Vissers, F. Smallenburg, M. Dijkstra, A. Imhof, and A. van Blaaderen, "Long-ranged oppositely charged interactions for designing new types of colloidal clusters," Phys. Rev. X **5**, 021012 (2015).

[107]D. Vella, E. du Pontavice, C. L. Hall, and A. Goriely, "The magneto-elastica: From self-buckling to self-assembly," Proc. R. Soc. A **470**, 20130609 (2014).

[108]C. Hall, D. Vella, and A. Goriely, "The mechanics of a chain or ring of spherical magnets," SIAM J. Appl. Math. **73**, 2029–2054 (2013).

[109]B. Kiani, D. Faivre, and S. Klumpp, "Elastic properties of magnetosome chains," New J. Phys. **17**, 043007 (2015).

[110]S. Klumpp, C. T. Lefèvre, M. Bennet, and D. Faivre, "Swimming with magnets: From biological organisms to synthetic devices," Phys. Rep. **789**, 1–54 (2019).

[111]H.-H. Boltz and S. Klumpp, "Buckling of elastic filaments by discrete magnetic moments," Eur. Phys. J. E **40**, 86 (2017).

[112]F. Deißenbeck, H. Löwen, and E. C. Oğuz, "Ground state of dipolar hard spheres confined in channels," Phys. Rev. E **97**, 052608 (2018).

[113]A. P. Philipse, M. P. B. van Bruggen, and C. Pathmamanoharan, "Magnetic silica dispersions: Preparation and stability of surface-modified silica particles with a magnetic core," Langmuir **10**, 92–99 (1994).

[114]A. P. Gast and L. Leibler, "Interactions of sterically stabilized particles suspended in a polymer solution," Macromolecules **19**, 686–691 (1986).

[115]G. Nägele, "On the dynamics and structure of charge-stabilized suspensions," Phys. Rep. **272**, 215–372 (1996).

[116]M. Eshraghi and J. Horbach, "Molecular dynamics simulation of charged colloids confined between hard walls: Pre-melting and pre-freezing across the BCC–fluid coexistence," Soft Matter **14**, 4141–4149 (2018).

[117]G. Filipcsei, I. Csetneki, A. Szilágyi, and M. Zrínyi, "Magnetic field-responsive smart polymer composites," Adv. Polym. Sci. **206**, 137–189 (2007).

[118]N. Frickel, R. Messing, and A. M. Schmidt, "Magneto-mechanical coupling in $CoFe_2O_4$-linked PAAm ferrohydrogels," J. Mater. Chem. **21**, 8466–8474 (2011).

[119]P. Ilg, "Stimuli-responsive hydrogels cross-linked by magnetic nanoparticles," Soft Matter **9**, 3465–3468 (2013).

[120]P. Cremer, H. Löwen, and A. M. Menzel, "Tailoring superelasticity of soft magnetic materials," Appl. Phys. Lett. **107**, 171903 (2015).

[121]P. Cremer, H. Löwen, and A. M. Menzel, "Superelastic stress–strain behavior in ferrogels with different types of magneto-elastic coupling," Phys. Chem. Chem. Phys. **18**, 26670–26690 (2016).

[122]G. Pessot, H. Löwen, and A. M. Menzel, "Dynamic elastic moduli in magnetic gels: Normal modes and linear response," J. Chem. Phys. **145**, 104904 (2016).

[123]V. Yannopapas, S. H. Klapp, and S. D. Peroukidis, "Magneto-optical properties of liquid-crystalline ferrofluids," Opt. Mater. Express **6**, 2681–2688 (2016).

[124]P. Cremer, M. Heinen, A. M. Menzel, and H. Löwen, "A density functional approach to ferrogels," J. Phys.: Condens. Matter **29**, 275102 (2017).

[125]S. Goh, A. M. Menzel, and H. Löwen, "Dynamics in a one-dimensional ferrogel model: Relaxation, pairing, shock-wave propagation," Phys. Chem. Chem. Phys. **20**, 15037–15051 (2018).

[126]A. M. Menzel, "Mesoscopic characterization of magnetoelastic hybrid materials: Magnetic gels and elastomers, their particle-scale description, and scale-bridging links," Arch. Appl. Mech. **89**, 17–45 (2019).

[127]M. Doi and S. F. Edwards, *The Theory of Polymer Dynamics* (Clarendon Press, Oxford, 1986).

[128]J. D. Jackson, *Classical Electrodynamics* (John Wiley & Sons, New Jersey, 2012).

[129]J. D. Weeks, D. Chandler, and H. C. Andersen, "Role of repulsive forces in determining the equilibrium structure of simple liquids," J. Chem. Phys. **54**, 5237–5247 (1971).

[130]J. Happel and H. Brenner, *Low Reynolds Number Hydrodynamics: With Special Applications to Particulate Media* (Springer Science & Business Media, The Netherlands, 2012).

[131]S. Kim and S. J. Karrila, *Microhydrodynamics: Principles and Selected Applications* (Courier Corporation, 2013).

[132]F. Balboa-Usabiaga, B. Kallemov, B. Delmotte, A. Bhalla, B. Griffith, and A. Donev, "Hydrodynamics of suspensions of passive and active rigid particles: A rigid multiblob approach," Commun. Appl. Math. Comput. Sci. **11**, 217–296 (2017).

[133]W. H. Press, B. P. Flannery, S. A. Teukolsky, and W. T. Vetterling, *Numerical Recipes* (Cambridge University Press Cambridge, 1989), Vol. 2.

[134]A. Daddi-Moussa-Ider, A. Guckenberger, and S. Gekle, "Long-lived anomalous thermal diffusion induced by elastic cell membranes on nearby particles," Phys. Rev. E **93**, 012612 (2016).

[135]A. Daddi-Moussa-Ider, M. Lisicki, and S. Gekle, "Mobility of an axisymmetric particle near an elastic interface," J. Fluid Mech. **811**, 210–233 (2017).

[136]A. Daddi-Moussa-Ider, "Diffusion of nanoparticles nearby elastic cell membranes: A theoretical study," Ph.D. thesis, University of Bayreuth, 2017.

[137]A. Daddi-Moussa-Ider and S. Gekle, "Brownian motion near an elastic cell membrane: A theoretical study," Eur. Phys. J. E **41**, 19 (2018).

[138]A. Daddi-Moussa-Ider, B. Rallabandi, S. Gekle, and H. A. Stone, "A reciprocal theorem for the prediction of the normal force induced on a particle translating parallel to an elastic membrane," Phys. Rev. Fluids **3**, 084101 (2018).

[139]W. Rudin, *Principles of Mathematical Analysis* (McGraw-Hill, New York, 1976), Vol. 3.

[140]K. Kumar, "On expanding the exponential," J. Math. Phys. **6**, 1928–1934 (1965).

[141]S. Timoshenko and Woinowsky-Krieger, *Theory of Plates and Shells* (McGraw-Hill, New York, 1959), Vol. 2.

[142]R. Bracewell, *The Fourier Transform and its Applications* (McGraw-Hill, Pennsylvania, 1999).

[143]D. V. Widder, *Laplace Transform (PMS-6)* (Princeton University Press, New Jersey, 2015).

[144]A. Sommerfeld, *Partial Differential Equations in Physics* (Academic Press, 1949), Vol. 1.

[145]M. Abramowitz and I. A. Stegun, *Handbook of Mathematical Functions* (Dover, New York, 1972), Vol. 5.